Electromagnetic interactions in a pair of coupled split-ring resonators

S. S. Seetharaman,* C. G. King, I. R. Hooper, and W. L. Barnes
Centre for Doctoral Training in Metamaterials, Department of Physics and Astronomy, University of Exeter, Stocker Road, Exeter EX4 4QL, United Kingdom
(Received 31 May 2017; revised manuscript received 1 August 2017; published 21 August 2017)

Split-ring resonators (SRRs) are a fundamental building block of many electromagnetic metamaterials. Typically the response of a metamaterial is assumed to be independent of interelement interactions in the material. We show that SRRs in close proximity to each other exhibit a rich coupling that involves both electric and magnetic interactions. We study experimentally and computationally the strength and nature of the coupling between two identical SRRs as a function of their separation and relative orientation. We characterize the electric and magnetic couplings and find that, when SRRs are close enough to be in each other's near field, the electric and magnetic couplings may either reinforce each other or act in opposition. At larger separations retardation effects become important.

DOI: 10.1103/PhysRevB.96.085426

I. INTRODUCTION

Ever since the publication of pioneering works by Pendry and Smith [1–3], metamaterials have emerged as a promising avenue for manipulating wave-matter interactions. There has been a continuously growing interest in the design and properties of their fundamental building blocks, the "meta-atoms" [4–8]. In many early works the response of the material was assumed to be independent of the interactions between the individual meta-atoms, but it was soon understood that this was not always the case. For example, Gay-Balmaz *et al.* [9] discovered that the response of a metamaterial consisting of split-ring resonators (SRRs) is not determined solely by the response of the individual resonators, but is also dependent on interelement interactions, which in turn depend upon the relative arrangement of the elements. Other reports in this area include those of Hesmer *et al.* (followed by others), who investigated SRR pairs in planar and axial orientations [10–19], Shamonina *et al.* and Shadrivov *et al.*, who studied the properties of chains of SRRs arranged along a common axis [20–23], and several studies investigating interactions in two- and three-dimensional arrays of SRRs [24–28].

In constructing complex metamaterial systems an understanding of the nature and strength of the interactions between the meta-atoms that make up the material is vital. Although it is well known that the electromagnetic coupling strength between SRRs depends on both their relative orientation and separation [9–19], the details of this interaction in both near- and far-field regimes has not been fully reported before. Here we provide a new and full characterization by investigating the coupling between a pair of axially oriented single-ring SRRs as a function of both their separation and relative orientation. Our approach will be helpful to understand the strength of interaction between any two SRRs in, for example, a one-dimensional (1D) chain of SRRs and can readily be extended to more complicated systems, where dense packing of meta-atoms may be important. Since single-ring SRRs exhibit bianisotropy, i.e., an incident electric field induces a magnetic dipole moment in addition to an electric dipole moment (and vice versa) [29], we must consider both electric and magnetic interactions. When we also include the additional degree of freedom arising from the relative orientation of the resonators, and the effect of retardation when the distance between the SRRs becomes of the order of the wavelength, it quickly becomes apparent that this seemingly simple system will exhibit quite a complex coupling landscape. We develop an analytical model that accounts for both the near-field interactions and the effect of phase retardation allowing us to predict the coupling strengths between arbitrarily oriented and separated resonators.

II. RESPONSE OF A SINGLE SRR AND AN AXIALLY COUPLED SRR PAIR

The single-ring SRR structure and its resonant response have been extensively discussed in the literature [29–39]. Consider an SRR illuminated by a plane wave, as in Fig. 1. The electric fields of the incident plane wave induce a circulating electric current around the ring with associated electric and magnetic dipole moments. The SRR will exhibit a resonant response, the resonant frequency being determined by the specific geometry of the SRR (the SRR can be considered as a simple LC resonator where the capacitance arises from charge separation across the split and the inductance arises from the circulating currents in the ring) [37,38]. In this section we will experimentally probe the response of a single SRR, and of two SRRs in close proximity having relative orientations of 0°, 90°, and 180°.

The SRRs for our experiment were fabricated from 1.6-mm-thick Duroid 5880 dielectric sheets clad with 20 μm of copper. Each SRR was designed to have an outer ring radius of 3.5 mm, a ring width of 370 μm, and a split-gap width of 1 mm designed to resonate at 5.8 GHz. A layer of photoresist was coated on top of the copper layer and the SRR design was written into the photoresist layer using a laser writer (Durham Magneto Optics Microwriter ML2). The resist was subsequently developed and etched using ferric chloride. The relative permittivity of the Duroid substrate, as taken from the data sheet, is $2.20 + 1.98 \times 10^{-3}i$ at 8 GHz.

For ease of experimentation the SRRs were placed in a rectangular waveguide, allowing for simple exploration of

*ss693@exeter.ac.uk

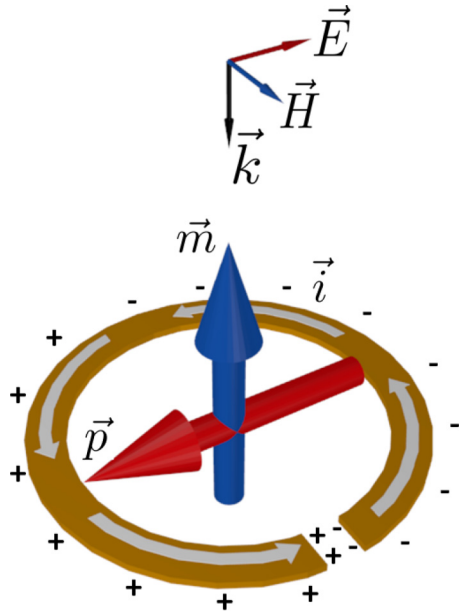

FIG. 1. Schematic of a split-ring resonator oriented with respect to an incident electromagnetic wave such that the electric field component of the wave is polarized across the split gap of the SRR. The corresponding induced electric and magnetic dipole moments in the SRR are shown as the red and the blue arrows, respectively. The arrows are indicative only of the polarizations of the induced dipole moments and not of their respective strengths or positions. The broken white arrow on the SRR surface indicates the electric current that is induced in the SRR.

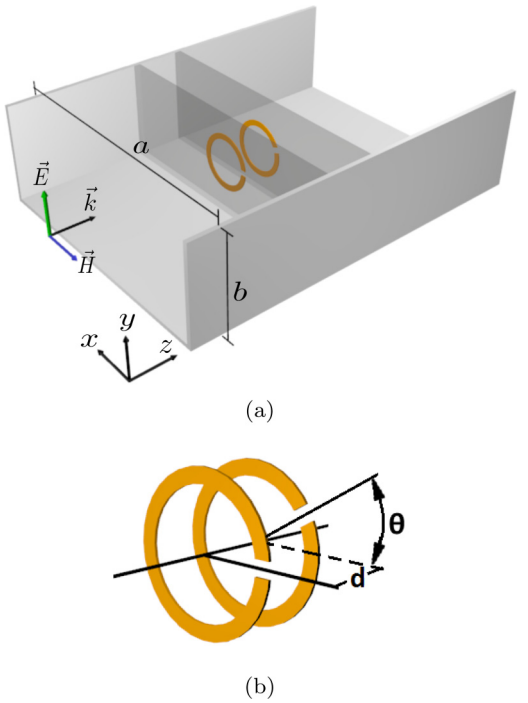

FIG. 2. (a) A schematic of the experimental setup showing the SRR pair within the rectangular waveguide with the lid removed. The substrates, shown as translucent blocks, face outwards in the experiment such that the only medium between the SRRs is air. The black arrow shows the direction of propagation $\vec{k}$ of the TE_{10} mode while the green and blue arrows indicate the orientation of the electric and magnetic fields of the mode, respectively. The length and breadth of the cross section of the waveguide are a and b, respectively. (b) The axially oriented SRR pair with a separation d and relative orientation θ.

the resonances of the systems through measurements of the reflection and transmission spectra obtained using a vector network analyzer (Anritsu VectorStar). In our experiments we used a customized C-band (WR137) waveguide with a detachable lid for ease of access and ease of arrangement of the SRRs. The low frequency cutoff of the TE_{10} mode for the WR137 waveguide is 4.3 GHz but, due to excessive absorptive losses within the guide close to this cutoff, the usable bandwidth is usually 5.35 to 8.2 GHz. The SRR's design resonance frequency of 5.8 GHz maximizes the frequency band over which we could observe the coupled modes of our system. We measured the response of our systems across the full frequency range for which the TE_{10} mode is the only mode supported by the waveguide.

The first SRR of the pair (or just the single SRR) was always oriented such that the electric field component of the TE_{10} mode was polarized across the split, as shown in Fig. 1. The second SRR was placed some distance behind the first such that the substrates are always facing outwards as shown in Fig. 2(a). The second SRR was rotated with respect to the first, as shown in Fig. 2(b). The reflection and transmission spectra were then collected. The measured reflected and transmitted intensities as a function of frequency for a single SRR are shown in Fig. 3(a), the resonant frequency of the fundamental mode is seen at 5.8 GHz. We note that the additional features evident in the spectra at low frequencies are likely to be due to losses when using the waveguide below its usual operational bandwidth. We subsequently introduced a second identical SRR 2 mm behind the first and measured the reflection and transmission spectra for the three relative rotation angles of 0°, 90°, and 180° [Figs. 3(b)–3(d)]. At this separation (2 mm) the SRRs are coupled strongly to each other via their near fields.

If two identical SRRs are in close proximity along a common axis the eigenmode of the single SRR will split into two new eigenmodes, one at a higher frequency and one at a lower frequency than the original, in the same manner as coupled resonators in other areas of physics. We can qualitatively understand the coupling mechanisms in the SRR pair for the different relative orientation angles by using a simple dipole model. In the simple case of two dipoles the strength of the coupling between the dipoles depends upon their relative orientation and the coupling can be either longitudinal or transverse in nature, as shown in Fig. 4. These coupled modes, whether longitudinal or transverse, correspond to aligned or anti-aligned dipole moments. For transversely coupled dipoles the symmetric mode (aligned dipole moments) is the higher frequency solution and the antisymmetric mode (anti-aligned dipole moments) is the lower frequency solution; for longitudinally coupled dipoles this situation is reversed. We also note that, for a given separation, the frequency difference between the coupled modes is greater for longitudinally coupled dipoles than for transversely coupled dipoles [40]. From Fig. 1 we note that the electric and magnetic dipole moments of a single SRR are orthogonal to each other so

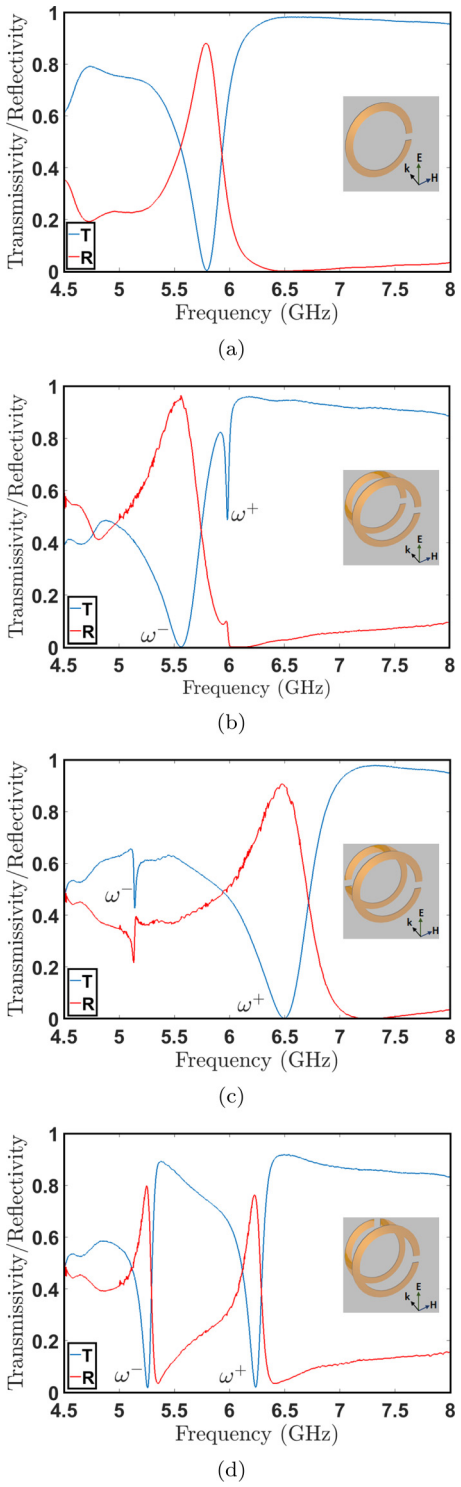

FIG. 3. Reflection and transmission spectra for a single SRR (a), and a pair of SRRs oriented with relative rotation angles of 0° (b), 180° (c), and 90° (d) when separated by a distance of 2 mm. The ω^- and ω^+ labels indicate the lower- and higher-frequency coupled modes, respectively. Insets: Schematics showing the relative orientations of the SRR pair and the incident electromagnetic wave.

that the coupling between a pair of axially oriented SRRs via their electric dipole moments will be transverse in nature, while the coupling via their magnetic dipole moments will be longitudinal.

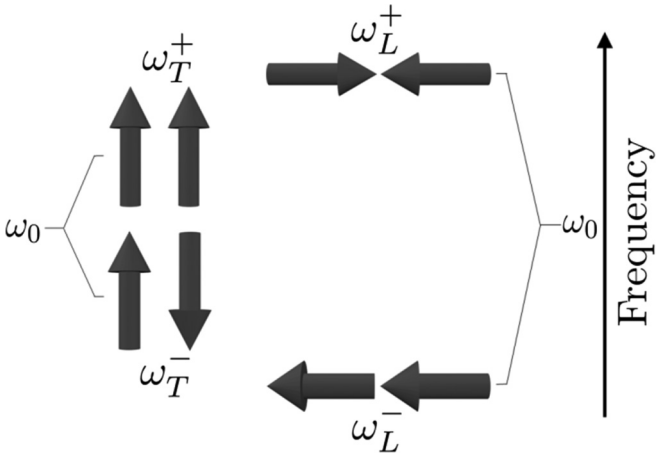

FIG. 4. A schematic showing the splitting of the coupled modes of a pair of dipoles for both transverse (left) and longitudinal (right) orientations of the dipole moments. The magnitude of the frequency splitting is larger when the dipoles are coupled longitudinally.

To explain the features in the spectra for the three relative rotations of the two SRRs it is instructive to consider the relative orientations of the electric and magnetic dipole moments for each case, as shown in Fig. 5. We begin by considering the pair of SRRs with a 0° rotation between them [Figs. 5(a) and 5(b)]. Since the electric dipole moments are transversely coupled and the magnetic dipole moments are longitudinally coupled, when the electric dipole moments are aligned (anti-aligned) and thus raise (lower) the mode's energy, the associated coupling via the magnetic moments acts to counter these changes [this can be seen by comparing Figs. 5(a) and 5(b) with Fig. 4]. Thus we might expect the frequency splitting between ω^+ and ω^- to be smaller than would be the case were it due to coupling via the electric or magnetic dipole moments alone. As we will see when we consider the other relative rotations, this is indeed the case.

We can also understand the strength of radiative coupling to the modes, and the relative strength of the coupling between the SRRs via the electric and magnetic dipole moments, in a similar way. In this geometry only the electric field of the incident radiation can excite the SRRs (the magnetic field is orthogonal to the magnetic dipole moments) so that we need only consider the net electric dipole moment of the SRR pair; if this is large then there will be strong coupling to radiation and we will observe a broad resonance, while if it is weak we will observe a narrow resonance. We can thus identify the ω^+ mode (narrow) as having anti-aligned electric dipole moments [Fig. 5(b)], and the ω^- mode (broad) as having aligned electric dipole moments [Fig. 5(a)]. By comparison with Fig. 4 we can also identify that the coupling between the SRRs via the magnetic dipole moments must be greater for this separation than coupling via the electric dipole moments.

When the second SRR in the pair is rotated such that $\theta = 180°$ the currents circulating around the second ring are reversed relative to the 0° rotated system for both coupled modes [Figs. 5(c) and 5(d)]. By referring to Fig. 4 we now see that the coupling between the SRRs via the electric dipole moments and the coupling via the associated magnetic dipole moments will act in concert; this results in a larger frequency splitting

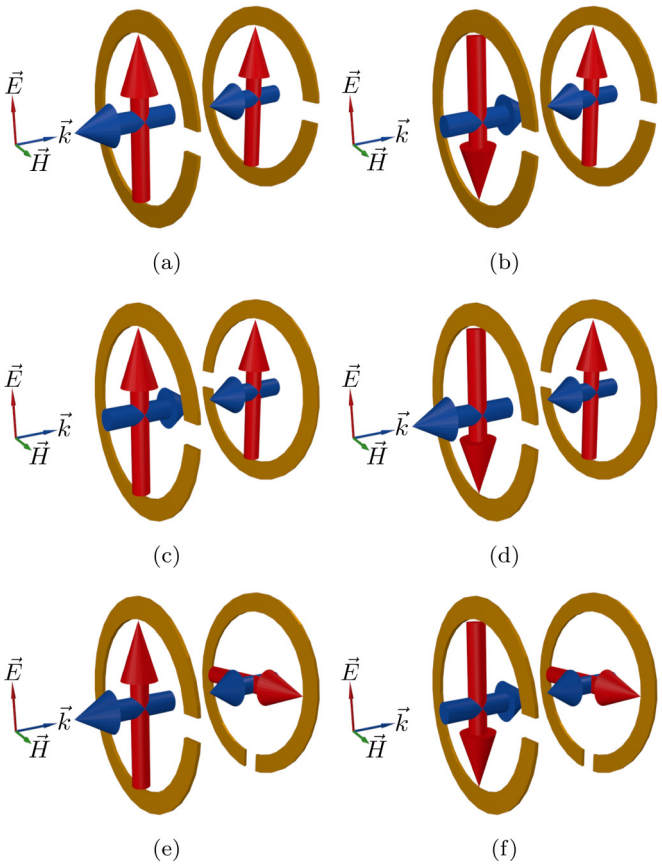

FIG. 5. The relative orientations of the transversely coupled electric dipole moments, and longitudinally coupled magnetic dipole moments, in the coupled SRR pairs for relative rotations of 0° [(a) and (b)], 180° [(c) and (d)], and 90° [(e) and (f)].

between the modes. The net electric dipole moment for the modes will be approximately the same as for the 0° rotated system, resulting in modes of similar widths, but, importantly, it is now the ω^- mode which is narrow and has anti-aligned electric dipole moments, while the ω^+ mode is broad.

The electric dipole moment corresponding to the fundamental mode of the single SRR is always polarized in the direction across the split gap (see Fig. 1). Therefore, for the final case when the relative orientation angle between the SRRs is $\theta = 90°$, the electric dipole moments of the two SRRs are orthogonal to each other so that the coupling between the SRRs is purely via their magnetic dipole moments [Figs. 5(e) and 5(f)]. Since there is no coupling via the electric dipole moments we expect the size of the frequency splitting to lie somewhere between that of the 0° and 180° cases, this can be seen from the data. Since the electric field of the incident radiation is aligned only with the electric dipole moment of the first SRR in the pair, the net electric dipole moment of the SRRs will be the same for both coupled modes, and their widths will be approximately equal, again, as observed.

III. ANALYTIC MODEL

From the previous section it is clear that, by using a simple toy model of interacting electric and magnetic dipoles, we can qualitatively understand the coupling mechanisms in a pair of axially oriented SRRs in close proximity to each other. However, it would be preferable to have a more complete analytical model that can accurately account for both near- and far-field interactions if we wish to understand the responses of these systems for different separations. Such a model can be developed by considering the Lagrangian for a pair of identical lossless resonators, and a complete treatment for their interactions in free space can be found in [15,41,42]; here we present the equations required to implement the model (a full derivation of the equations is presented in the Supplemental Material [43]).

The interaction energies between a pair of identical conducting elements arising from their current $W_{J,ij}$ and charge $W_{q,ij}$ distributions are given by

$$W_{J,ij} = \int d^3\mathbf{r} \int d^3\mathbf{r}' \mu_0 \mathbf{J}^*(\mathbf{r}) \underline{\underline{G}}(\mathbf{r},\mathbf{r}') \mathbf{J}(\mathbf{r}'),$$
$$W_{q,ij} = \int d^3\mathbf{r} \int d^3\mathbf{r}' \frac{1}{\epsilon_0} q^*(\mathbf{r}) g(\mathbf{r},\mathbf{r}') q(\mathbf{r}'), \quad (1)$$

where $\mathbf{J}$ and q are the current and charge density distributions of the fundamental eigenmode of a single element (in our case a single SRR within the waveguide), and $\underline{\underline{G}}(\mathbf{r},\mathbf{r}')$ and $g(\mathbf{r},\mathbf{r}')$ are the tensor Green's and the scalar Green's functions, respectively. When $i = j = 1$, these terms correspond to the self-energies of a single element, and when $i \neq j$ they correspond to mutual-energy terms.

The components of the Green's tensor within a rectangular waveguide are given by (see the Supplemental Material [43])

$$G_{xx} = \sum_{m=0}^{\infty}\sum_{n=1}^{\infty} i \frac{\epsilon_m \epsilon_n}{2abk_I} \cos\left(\frac{m\pi x'}{a}\right)\sin\left(\frac{n\pi y'}{b}\right) \times \cos\left(\frac{m\pi x}{a}\right)\sin\left(\frac{n\pi y}{b}\right) e^{ik_I|z-z'|},$$
$$G_{yy} = \sum_{m=1}^{\infty}\sum_{n=0}^{\infty} i \frac{\epsilon_m \epsilon_n}{2abk_I} \sin\left(\frac{m\pi x'}{a}\right)\cos\left(\frac{n\pi y'}{b}\right) \times \sin\left(\frac{m\pi x}{a}\right)\cos\left(\frac{n\pi y}{b}\right) e^{ik_I|z-z'|},$$
$$G_{zz} = \sum_{m=1}^{\infty}\sum_{n=1}^{\infty} i \frac{\epsilon_m \epsilon_n}{2abk_I} \sin\left(\frac{m\pi x'}{a}\right)\sin\left(\frac{n\pi y'}{b}\right) \times \sin\left(\frac{m\pi x}{a}\right)\sin\left(\frac{n\pi y}{b}\right) e^{ik_I|z-z'|}, \quad (2)$$

where

$$\epsilon_m = \begin{cases} 1, & m = 0, \\ 2, & m > 0 \end{cases} \quad (3)$$

and k_I is the component of the wave vector along the waveguide,

$$k_I^2 = k_0^2 - \left(\frac{m\pi}{a}\right)^2 - \left(\frac{n\pi}{b}\right)^2, \quad (4)$$

where $k_0 = \omega_0/c$ is the free-space wave vector corresponding to the natural resonant frequency of the split rings. This is a natural choice because the SRRs excite each other via their radiated fields the strongest, at their resonant frequency. m and n are non-negative integers corresponding to the supported

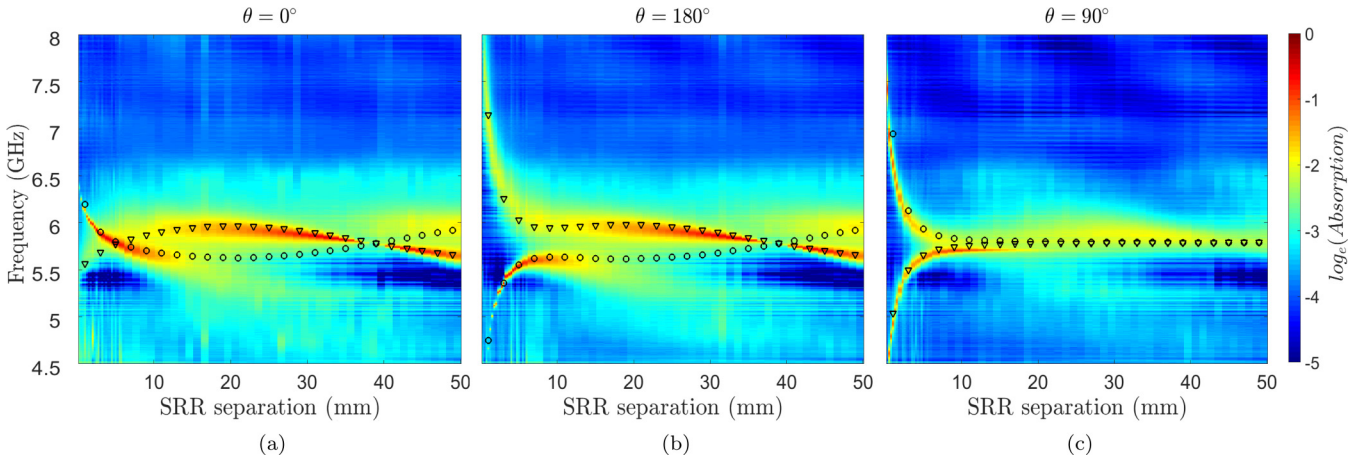

FIG. 6. The absorption by the SRR pair as calculated from the measured reflection and transmission spectra plotted on a color scale (see color bar) as a function of the separation between the SRRs, for relative rotation angles of (a) 0°, (b) 180°, and (c) 90°. The black circles indicate the position of the antisymmetric resonant mode and the black triangles represent the symmetric resonant mode of the systems as predicted by the analytic model.

modes of the empty waveguide, and a and b are the length and breadth of the waveguide's cross section, respectively, as shown in Fig. 2(a). The scalar Green's function $g = G_{zz}$.

The resonant frequencies of the symmetric and antisymmetric modes of the coupled system can then be calculated [15] using

$$\omega_s = \omega_0\sqrt{\frac{1+\beta}{1+\alpha}},$$
$$\omega_{as} = \omega_0\sqrt{\frac{1-\beta}{1-\alpha}}, \tag{5}$$

where ω_0 is the resonant frequency of a single SRR, and the magnetic (α) and electric (β) interaction constants due to the current and charge distributions, respectively, are given by [15],

$$\alpha = \frac{W_{J,12}}{W_{J,11}},$$
$$\beta = \frac{W_{q,12}}{W_{q,11}}. \tag{6}$$

To calculate the $\mathbf{J}$ and q distributions of the fundamental eigenmode of a single SRR that are needed as input for this model we used the eigensolver of a commercial finite-element software package (Comsol Multiphysics).

IV. THE COUPLED MODES OF AXIALLY ORIENTED SRR PAIRS AS A FUNCTION OF RELATIVE ORIENTATION AND SEPARATION

Next we consider in more detail the coupled modes of a pair of axially oriented SRRs as a function of orientation and separation. Reflection R and transmission T spectra were experimentally recorded as described in Sec. II, for relative orientations of 0°, 90°, and 180° as a function of the separation between the SRRs. Absorption spectra were calculated using (1-R-T) and are shown in Fig. 6, together with the positions of the resonant frequencies predicted by the analytical model. In Fig. 7 we plot the real parts of the coupling coefficients α and β as obtained from the model, which represent the strength of coupling between the SRRs due to the current distributions (the electrodynamic contribution), and the charge distributions (the electrostatic contribution) respectively.

The three different data sets shown in Fig. 6 exhibit some common features. For separations above ~5 mm the modes are only weakly dependent on separation while for small separations the mode frequencies diverge. We begin by looking at the large separation data.

For both $\theta = 180°$ and $\theta = 0°$, when the separation is greater than ~20 mm very similar behavior is exhibited; in this regime near-field interactions between the SRRs are absent. The analytical model predicts the presence of the antisymmetric mode between 15 and 40 mm despite the mode being absent in the experimental data. The mode may not be visible because of its poor coupling to the incident radiation at these separations, but it is still an eigenmode of the system and is predicted by the analytical model. From Eq. (5) we see that when the coupling coefficients are comparable the resonant modes become degenerate, while when these coefficients are markedly different the splitting is strong. At these large separations the interaction is mediated solely by the propagating field in the waveguide, and this interaction will oscillate as a function of separation with a period corresponding to the wavelength within the waveguide, i.e., in this regime the interaction is retarded.

When $\theta = 90°$ things are somewhat different. From Figs. 6(c) and 7(c), we see that the resonant modes of the SRR pair are degenerate and take the same frequency as the resonant frequency of an individual SRR. The lack of any oscillatory behavior similar to that in the $\theta = 0°$ and $\theta = 180°$ cases results from the electric dipole moments of the individual rings being orthogonal (the electric polarization of the fields radiated by the first SRR cannot excite the electric dipole moment of the second SRR). In essence the effect of retardation has been switched off in this geometry so that any interactions may only occur via the near fields.

We now turn to the small separation regime. When $\theta = 0°$, the near-field coupling mediated via the charge and current

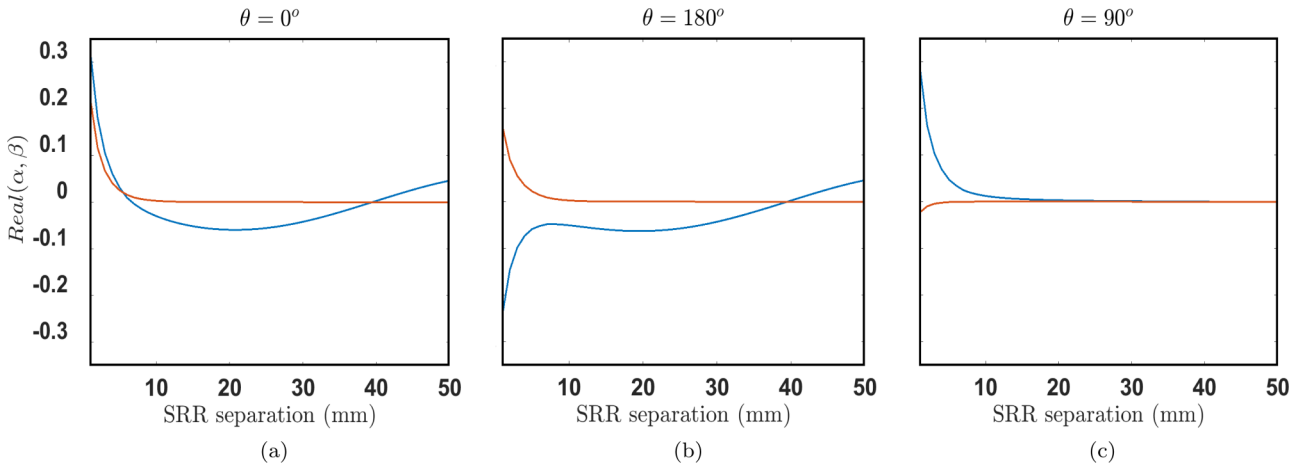

FIG. 7. The coupling coefficients between the SRRs arising due to the currents (α) and electric charges (β) for relative rotation angles of (a) 0°, (b) 180°, and (c) 90°, as a function of SRR separation. The blue curves represent the real part of α and the red curves that of β in all three plots.

distributions conflict each other (the values of α and β have the same sign), see Fig. 7(a). This is due to the electric dipole moments and the magnetic dipole moments of the SRRs both being aligned or anti-aligned [Figs. 5(a) and 5(b)], and results in a relatively small frequency splitting. We also note that at small separations the magnitude of α is greater than that of β indicating that the coupling strength between the SRRs due to the magnetic dipole moments is greater than that due to the electric dipole moments, confirming our prediction in Sec. II. This, coupled with the fact that, for this orientation, the near-field contribution to α has the opposite sign to the radiative contribution, results in a crossing in the values of α and β, and a corresponding mode crossing in Fig. 6(a) at a separation of approximately 6 mm.

When $\theta = 180°$, the near-field contributions to α reverse their sign relative to the $\theta = 0°$ case. The near-field coupling mediated via the charge and current distributions act in concert (the values of α and β have opposite signs), see Fig. 7(b). Physically, as described in Sec. II, this difference in sign arises due to the difference in relative alignment of the electric and magnetic dipole moments [Figs. 5(c) and 5(d)]. Since the coupling via the electric dipole moments is transverse in nature, while that of the magnetic dipole moments is longitudinal, this results in a significant splitting of the resonant modes. We also note that the contribution to α arising from near-field interactions has the same sign as that of the radiative contribution, and there is thus no frequency crossing of the coupled modes at these small separations.

Lastly, for $\theta = 90°$, the dipole model discussed in Sec. II predicts the SRR interaction to be mediated only via the magnetic fields due to the orthogonal electric dipole moments of the two SRRs. However, we note from Fig. 7(c) that the electrostatic interaction is not completely absent at very close proximity. The coupled dipole model does not account for such near-field effects. The interaction in this case is mediated only by the decaying near fields, with the value of β too small to play a deciding role in the overall coupling. The extent of the mode splitting in the near-field regime is thus dominated by the fields arising from the currents oscillating around the SRRs.

The real parts of the coupling coefficients quantify the strength of each type of interaction and have been used to analyze the changing resonant response of coupled SRRs. The imaginary parts of the coupling coefficients represent damping and are important for predicting the line shapes of the resonant modes, which is the subject of a future study.

V. CONCLUSION

We have studied the coupled modes of a pair of identical split-ring resonators as a function of their separation and relative orientation. We placed the SRRs in a rectangular waveguide and measured their reflection and transmission spectra, and used an analytical model to help build an understanding of the physical mechanisms involved. We have shown that the coupling in such systems exhibits a rich behavior that can only be understood by considering near-field and far-field interactions of both electric and magnetic character. Our results will help inform the design of more complex metamaterials that incorporate SRRs into arrays where the strength of inter-resonator coupling becomes significant, as, for example, in the case of very dense arrays.

All data created during this research are openly available in Ref. [44].

ACKNOWLEDGMENTS

We acknowledge financial support from the Engineering and Physical Sciences Research Council (EPSRC) of the United Kingdom, via the EPSRC Centre for Doctoral Training in Metamaterials (Grant No. EP/L015331/1). We thank Dr. David Powell, Non-linear Physics Centre, Australian National University for valuable discussions in relation to his work.

[1] J. B. Pendry, A. J. Holden, D. J. Robbins, and W. J. Stewart, J. Phys.: Condens. Matter **10**, 4785 (1998).

[2] J. B. Pendry, A. J. Holden, D. J. Robbins, and W. J. Stewart, IEEE Trans. Microw. Theory Tech. **47**, 2075 (1999).

[3] D. R. Smith, W. J. Padilla, D. C. Vier, S. C. Nemat-Nasser, and S. Schultz, Phys. Rev. Lett. **84**, 4184 (2000).

[4] E. Shamonina and L. Solymar, J. Magn. Magn. Mater. **300**, 38 (2006).

[5] C. E. Kriegler, M. S. Rill, S. Linden, and M. Wegener, IEEE J. Sel. Top. Quantum Electron. **16**, 367 (2010).

[6] N. I. Zheludev and Y. S. Kivshar, Nat. Mater. **11**, 917 (2012).

[7] G. R. Keiser, K. Fan, X. Zhang, and R. D. Averitt, J. Infrared Millim. Terahertz Waves **34**, 709 (2013).

[8] N. Meinzer, W. L. Barnes, and I. R. Hooper, Nat. Photon. **8**, 889 (2014).

[9] P. Gay-Balmaz and O. Martin, J. Appl. Phys. **92**, 2929 (2002).

[10] F. Hesmer, E. Tatartschuk, O. Zhuromskyy, A. A. Radkovskaya, M. Shamonin, T. Hao, C. J. Stevens, G. Faulkner, D. J. Edwards, and E. Shamonina, Phys. Status Solidi B **244**, 1170 (2007).

[11] N. Liu, S. Kaiser, and H. Giessen, Adv. Mater. **20**, 4521 (2008).

[12] N. Liu, H. Liu, S. Zhu, and H. Giessen, Nat. Photon. **3**, 157 (2009).

[13] T. Q. Li, H. Liu, T. Li, S. M. Wang, J. X. Cao, Z. H. Zhu, Z. G. Dong, S. N. Zhu, and X. Zhang, Phys. Rev. B **80**, 115113 (2009).

[14] N. Feth, M. König, M. Husnik, K. Stannigel, J. Niegemann, K. Busch, M. Wegener, and S. Linden, Opt. Express **18**, 6545 (2010).

[15] D. A. Powell, M. Lapine, M. V. Gorkunov, I. V. Shadrivov, and Y. S. Kivshar, Phys. Rev. B **82**, 155128 (2010).

[16] D. A. Powell, K. Hannam, I. V. Shadrivov, and Y. S. Kivshar, Phys. Rev. B **83**, 235420 (2011).

[17] C. Tang, Q. Wang, F. Liu, Z. Chen, and Z. Wang, Opt. Express **21**, 11783 (2013).

[18] S. M. Hein and H. Giessen, Phys. Rev. B **91**, 205402 (2015).

[19] P. C. Wu, W. Hsu, W. T. Chen, Y. Huang, C. Y. Liao, A. Q. Liu, N. I. Zheludev, G. Sun, and D. P. Tsai, Sci. Rep. **5**, 9726 (2015).

[20] E. Shamonina, V. A. Kalinin, K. H. Ringhofer, and L. Solymar, Electron. Lett. **38**, 371 (2002).

[21] E. Shamonina, V. A. Kalinin, K. H. Ringhofer, and L. Solymar, J. Appl. Phys. **92**, 6252 (2002).

[22] I. V. Shadrivov, A. N. Reznik, and Y. S. Kivshar, Physica B: Condens. Matter **394**, 180 (2007).

[23] A. Radkovskaya, O. Sydoruk, M. Shamonin, E. Shamonina, C. J. Stevens, G. Faulkner, D. J. Edwards, and L. Solymar, IET Microwav. Antennas Propag. **1**, 80 (2007).

[24] H. Liu, D. A. Genov, D. M. Wu, Y. M. Liu, Z. W. Liu, C. Sun, S. N. Zhu, and X. Zhang, Phys. Rev. B **76**, 073101 (2007).

[25] N. Liu and H. Giessen, Opt. Express **16**, 21233 (2008).

[26] I. Sersic, M. Frimmer, E. Verhagen, and A. F. Koenderink, Phys. Rev. Lett. **103**, 213902 (2009).

[27] M. Lapine, D. Powell, M. Gorkunov, I. Shadrivov, R. Marqués, and Y. Kivshar, Appl. Phys. Lett. **95**, 084105 (2009).

[28] M. Decker, S. Linden, and M. Wegener, Opt. Lett. **34**, 1579 (2009).

[29] R. Marqués, F. Medina, and R. Rafii-El-Idrissi, Phys. Rev. B **65**, 144440 (2002).

[30] J. E. Allen and S. E. Segre, Il Nuovo Cimento Series 10 **21**, 980 (1961).

[31] A. Radkovskaya, M. Shamonin, C. J. Stevens, G. Faulkner, D. J. Edwards, E. Shamonina, and L. Solymar, Microw. Opt. Technol. Lett. **46**, 473 (2005).

[32] J. Zhou, T. Koschny, M. Kafesaki, E. N. Economou, J. B. Pendry, and C. M. Soukoulis, Phys. Rev. Lett. **95**, 223902 (2005).

[33] L. Zhou and S. T. Chui, Phys. Rev. B **74**, 035419 (2006).

[34] J. Du, S. Liu, Z. Lin, and S. T. Chui, J. Appl. Phys. **104**, 014907 (2008).

[35] L. Zhou, X. Huang, Y. Zhang, and S. T. Chui, Mater. Today **12**, 52 (2009).

[36] M. Labidi, J. B. Tahar, and F. Choubani, J. Mater. Sci. Eng. B **1**, 696 (2011).

[37] L. J. Roglá, J. Carbonell, and V. E. Boria, IET Microw. Antennas Propag. **1**, 170 (2007).

[38] O. Sydoruk, E. Tatartschuk, E. Shamonina, and L. Solymar, J. Appl. Phys. **105**, 014903 (2009).

[39] L. Solymar, *Waves in Metamaterials* (Oxford University Press, Oxford, 2008).

[40] N. Liu, Physik J. **9**, 57 (2010).

[41] M. Liu, D. A. Powell, I. V. Shadrivov, and Y. S. Kivshar, Appl. Phys. Lett. **100**, 111114 (2012).

[42] E. Tatartschuk, N. Gneiding, F. Hesmer, A. Radkovskaya, and E. Shamonina, J. Appl. Phys. **111**, 094904 (2012).

[43] See Supplemental Material at http://link.aps.org/supplemental/10.1103/PhysRevB.96.085426 for the full derivation of the Green's function for the Helmholtz equation in a rectangular waveguide.

[44] University of Exeter's institutional repository, http://hdl.handle.net/10871/28937.